Sensors and Actuators A 326 (2021) 112733

Contents lists available at ScienceDirect

Sensors and Actuators A: Physical

journal homepage: www.elsevier.com/locate/sna

Fabrication and characteristic study on mixing enhancement of a magnetofluidic mixer

Ran Zhou*, Athira Surendran, Jingyang Wang

Department of Mechanical and Civil Engineering, Purdue University Northwest, 2200 169th St. Hammond, IN 46323, USA

ARTICLE INFO

Article history:
Received 11 February 2021
Received in revised form 11 March 2021
Accepted 30 March 2021
Available online 5 April 2021

Keywords:
Mixing enhancement
Microfluidics
Magnetic field
Ferrofluid
Experiment and simulation
Biomedical engineering

ABSTRACT

The needs for fast mixing of two miscible fluids in microfluidic device is increasing recently and has been widely used for DNA synthesis, clinic diagnostics and chemical reaction. However, the mixing at microscale relies heavily on slow molecular diffusion because of its low Reynolds number and thus laminar flow. In this work, therefore, a magnetofluidic mixer with the integration of magnetic field is presented for rapid mixing between ferrofluid and distilled water with no harmful Joule heat generated. Parametric study of experiment and simulation was performed to discuss the effect of flow rate, placement angle of magnet and width of magnet on the mixing efficiency between two fluids. It was found that the mixing performance of 0.76 was the most homogeneous when the angle $\alpha = 1/12\pi$ because of the acceleration-deceleration couples (ADC) and mass conservation law. It was also found that the mixing performance increases from 0.13 to 0.49 as the magnet width increases from $w_m = 50\,\mu$m to $w_m = 250\,\mu$m while decreases when magnet width is wider than $w_m = 250\,\mu$m due to local reduced Peclet number. The developed micromixer and mixing mechanism will be of great potentials and insight for future quick optimization of biomedical and chemical mixing devices.

Published by Elsevier B.V.

1. Introduction

Since the discovery of microfluidics in the 1980s, many theories have been formulated regarding the mechanism allowing fluid and particle manipulation on a micro scale [1–4]. The applications of microfluidics range from micromechanics, micro thermal technologies to biomedical sciences [5–10]. The biomedical field especially takes great advantage of the mechanisms in microfluidics to perform various applications such as drug delivery [11–14], clinical diagnostics [15–18] and point of care diagnostics [19–22]. A diverse range of experimentation can be executed in microfluidic systems and the most common function for biomedical field are mixing of reagents and detection, sorting and separation of microparticles, where mixing of reagents has been proved to be crucial for pre-processing, enzyme assays, cell lysis and protein folding [23–29]. Although the high volume to surface area ratio is beneficial, a small Reynolds number (Re < 1) prevails in microfluidic devices because of the small channel dimension, which leads to a laminar flow regime. Hence, homogeneous mixing in microfluidic systems can only be achieved through molecular diffusion, which consumes time and requires long channel lengths and large sample sizes. Thus, the techniques of rapid mixing has been widely developed to increase mixing performance and achieve homogeneous mixture efficiently [30–35].

Numerous studies have been conducted to develop various microscale mixers with enhanced mixing performance and can be categorized into active and passive micromixers. Passive micromixers rely on the geometry of the channels and hydrodynamic driving force from the fluids to create a homogeneous mixture. This technique does not require an external force or field but generally requires longer reaction time and longer channel lengths due to the slow mixing performance [36–38]. Shi et al. [39] presented a serpentine micromixer for the activation of amino acids with the integration of ellipsoidal grooves embedded to the serpentine square wave walls that produced vortex which in turn increased the mixing efficiency. The proposed square wave serpentine channel with grooves yielded a mixing performance of 40% at eight units compared to 18% for serpentine channel without grooves. In this work, the improved channel was applied as a micromixing reactor for carboxyl activation and for in-situ polypeptide synthesis. On the other hand, active mixing schemes utilize external forces and fields such as electrical, acoustic, thermal and magnetic forces to promote homogeneous mixing and form a miscible fluid. Nazari et al. [40] developed a novel electrokinetic micromixer

* Corresponding author.
E-mail address: zhou970@pnw.edu (R. Zhou).
URL: https://www.pnw.edu/people/ran-zhou-ph-d/ (R. Zhou).

https://doi.org/10.1016/j.sna.2021.112733
0924-4247/Published by Elsevier B.V.

by incorporating conductive surfaces to induce mixing. Different geometries of mixing chambers and number of conductive surfaces were analyzed to observe the effect on mixing and mass transfer. For all the results, turbulence occurred in the midst of flow in the mixing chamber to agitate the fluids and the highest mixing degree of 95% was achieved. Rasouli et al. [41] designed a sustainable acoustic micromixer for rapid mixing that converts acoustic energy generated by oscillatory bubbles into chaotic eddy and acoustic microstreams. The proposed method was applied in the synthesis of organic nanoparticles (polymeric nanoparticles and nanoliposomes) because of the enhanced mixing time and nucleation environment, which controls the nanoprecipitation process. Active micromixing have also been explored in thermal mixing, for instance Ajarostaghi et al. [42] incorporated micromixers to induce thermal mixing and cooling between two miscible liquids with different temperatures by integrating a porous media. A two-dimensional Lattice Boltzmann model was utilized to run this numerical study and it was found that thermal mixing and cooling performance enhanced by increasing the aspect ratio of the porous media and decreasing the porosity and thermal conductivity of the porous block.

Magnetic field has been utilized widely to improve mixing efficiency because of the high performance exhibited by strong magnetic fields and its gradient. Generally, magnetic fields can be generated at a lower cost compared to other active methods. Nouri et al. [43] performed numerical and experimental study on the mixing of ferrofluid and distilled water in a Y-shaped micromixer with the aid of a permanent magnet that generates a uniform magnetic field. In this study, the effects of intensity of magnetic field, concentration of ferrofluid nanoparticles and the flow rates were varied for parametric study. This investigation is the basis for most magnetic mixing studies as it clearly indicated the effects of different parameters with the presence of a magnetic field. Numerical methods have been employed in many studies to completely and thoroughly understand the fluid mixing mechanism. Wang et al. [44] numerically investigated the mixing performance of magnetic particles and buffer solution in the presence of alternating magnetic actuation sourced from electromagnets. The electromagnets were placed on both sides of the microchannel and generate alternating magnetic fields, creating chaotic flow in the microchannel which oscillates the magnetic microparticles to move to each side of the microchannel alternately while flowing in the streamwise direction. Liosis et al. [45] performed a numerical study on the mixing of wastewater and magnetic particles because magnetic particles can be used to trap metal ion impurities in wastewater. This study investigated the parameters that affect the distribution of magnetic particles throughout the microduct. A three-dimensional model was created and the concentration of magnetic nanoparticles were analyzed to determine the mixing performance. Kumar et al. [46] investigated a numerical model for a magnetofluidic mixer that simulated the mass transport of ferrofluid and fluorescent dye in the midst of sheath flow deionized water with the presence of nonuniform magnetic field. This work considered a two-dimensional model with a shallow depth to compensate for the three-dimensional effect to ensure that the results are accurate. The magnet was modeled above the channel and the results showed that the core stream of the ferrofluid and dye transported towards the upper sheath at the outlet. This is because magnetoconvective secondary flow increased the transport of nonmagnetic fluorescent dye towards the upper sheath. The results were compared to the experimental study for validation [47].

In this study, we performed an experimental and numerical study on the rapid mixing of ferrofluid and distilled water in a magnetofluidic micromixer containing a microchannel and an in-house fabricated micromagnet array. The micromagnet array is manufactured with a mixture of polydimethylsiloxane (PDMS) and

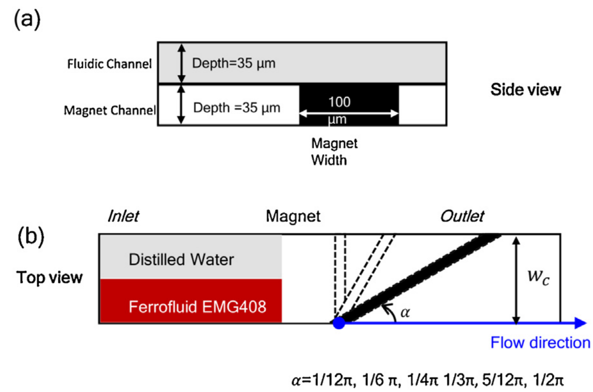

Fig. 1. Schematic illustration of mixing device. (a) is side view of mixing device. Flow direction is from left to right in fluidic channel. (b) is top view of micromixer and indicates the flow distribution in fluidic channel. The depth of both fluidic channel and magnet channel are the same and Depth = 35 μm. The width of the microfluidic channel is $w_c = 1000\,\mu$m. α is the angle between magnet and flow direction.

neodymium (NdFeB) powder and located on a different plane compared to the microchannel. The microscale magnet generates a strong magnetic field that imparts strong magnetic forces onto the magnetic nanoparticles present in the ferrofluid which promotes rapid mixing between the ferrofluid and distilled water. The microfluidic device was fabricated using soft-lithography for the experimental study because of the low-cost and efficiency of the technique. Parametric study was conducted where the total flow rate of the incoming fluids was varied. Experimental study was modeled to validate the results from the simulation and the results from both studies correlate well with each other. This validation provides fundamental support to simulate the effect of magnet angle and width, and overcome the difficulties of complex fabrication process. This study exhibits the experimental and numerical study of an interesting phenomenon that occurs with the magnetic field imposed by the micromagnets located on a different plane compared to the microchannel. Microscale magnets and ferrofluid are suitable for mixing of biological reagents because no harmful waves are emitted and ferrofluid is biocompatible.

2. Materials and methods

Fig. 1(a) is the front view of micromixer and demonstrates the dimension of fluidic channel and magnet channel. The depth of fluidic channel is Depth = 35 μm and is the same with that of magnet channel, which equals to the thickness of photoresist. The width of magnet in base case is $w_m = 100\,\mu$m and varies in numerical study in the following section. The width of the microfluidic channel is $w_c = 1000\,\mu$m. Fig. 1(b) is the top view the microfluidic mixer. In the experiment and simulation, distilled water was injected from the upper half of fluidic channel while ferrofluid with magnetic nanoparticle concentration of 1.2% (v/v) (EMG 408, Ferrotec) was injected from the lower half. The experiments were conducted with the constant flow ratio of 1 for a wide range of total flow rates from 0.2 to 4 mL/h. The magnet is placed directly below fluid flow and generates magnetic field causing mixing between two streams. The angle α between the magnet and flow direction varies from $\alpha = 1/12\pi$, $\alpha = 1/6\pi$, $\alpha = 1/4\pi$, $\alpha = 1/3\pi$, $\alpha = 5/12\pi$ to $\alpha = 1/2\pi$ in this work and the corresponding mixing performance will be discussed accordingly. The major differences between current work and previous research reside in the mixer and magnet designs. Compared with our previous single layer mixer where the magnet is placed hundreds of microns away from fluidic channel [24], the microfluidic mixer established in current work is two planes (top and bottom) and enables the direct contact between fluid and magnet, which maximized the impact of magnetic force on the mixing between two fluids. Standard experimental system and components [24] for microfluidics were applied in this work. The microfluidic device was placed on an inverted microscope (Amscope IN300TC-FL) platform. The high speed camera (Photron AX100) was mounted to microscope and used to record the flow phenomenon inside microfluidic channel. Two syringe pumps (Cole Parmer 74900) were applied to control the flow from each inlet separately. One millimeter syringe was installed on the pump to maximize the stability of fluid flow.

Fig. 2 indicates the fabrication of the magnetofluidic mixer. A low cost customized soft lithography method was applied to fabricate the high resolution microfluidic device [48,49]. A 2 × 3 inch rectangular smooth copper plate was placed on a 4 × 5 inch rectangular laminator sheet and a piece of photoresist film was then cut into a dimension of 3 × 4 inch. The photoresist film is protected by two clear films on the front and back, thus before positioning the photoresist film on top of the copper plate, the back clear film was carefully removed, which enables the photoresist film to bond with the copper plate and laminator sheet temporarily. The three items were then passed through a low-cost thermal laminator at 100 °C for three times in the forward orientation and three times in the backward orientation to ensure good adhesion and no bubbles formed between the photoresist film and the copper plate. After lamination, the front clear film attached to the photoresist film was removed carefully by hand. A negative photomask (10,000 dpi, CAD/Art Services) was aligned and placed on the processed copper plate. Then, the copper plate was exposed to ultraviolet (UV) light for 30 s and placed in the dark for one hour for the exposed photoresist to crosslink onto the copper plate. After the resting period, the exposed copper plate-photoresist film was developed in a sodium bicarbonate solution at 35 °C with a ratio of 100:1 of distilled water:sodium carbonate solution. During the developing process, the unexposed portion of the photoresist film was dissolved into the solution and the exposed pattern remained on the copper plate due to the crosslinked bond. The finished copper plate can be used as a master mold to fabricate multiple microfluidic structures. To complete the microfluidic device, the copper mold was first placed in an aluminum foil box. 25 g PDMS and 2.5 g PDMS activator (SYLGARD^{TM}184 Silicone Elastomer Kit, Dow Inc.) were mixed thoroughly, then placed inside a vacuum chamber to extract all the bubbles. After all the bubbles dissipated from the mixture, it is poured into the aluminum foil box where the copper mold was placed and box was then place in the oven, where the mixed PDMS was thermally cured for 2 h at 70 °C. After that, the cured PDMS was peeled away from the copper mold and this layer is called the ‘fluidic chip’ and used as the channel to mix different fluids. The above fabrications steps were repeated again with a different patterned negative photomask to fabricate the microstructures for the microscale magnetic array. After the ‘magnet chip’ was obtained, a 2 × 3 in rectangular glass and the ‘magnet chip’ were cleaned using isopropyl alcohol (IPA), distilled water, compressed air and adhesive tape in order to ensure no dust or contaminants were left on the surfaces. Oxygen plasma treatment was subjected onto both the glass and ‘magnet chip’ to promote adhesion and the surfaces were bonded and placed on a heated plate for 12 h at 120 °C. To fabricate the magnetic filling for the magnetic channel, 10 g PDMS base, 1 g PDMS activator and 11 g NdFeB powder (Magnequench, MQFP-B-20076) were mixed thoroughly and degassed. The mixture was then injected into the bonded ‘magnet chip’ at a low flow rate until the mixture filled the entire array. After that, the ‘magnet chip’ was baked in the oven at for 15 min at 120 °C for fast curing, followed by 2 h at 70 °C for complete curing. After the magnet was cured, it was permanently magnetized in the impulse magnetizer (IM 10, ASC Scientific). Before bonding the fluidic chip with the microscale magnetic channel, they were both cleaned thoroughly using IPA, distilled water, compressed air and adhesive tape. Oxygen plasma treatment was subjected onto both surfaces and the device was then placed on the heated plate for 12 h at 120 °C for firm bonding.

Table 1
EDS element detection in microscale magnet.

Element number	Element symbol	Element name
8	O	Oxygen
14	Si	Silicon
5	B	Boron
26	Fe	Iron
60	Nd	Neodymium

To validate the content of the microscale magnetic array, an energy dispersive spectroscopy (EDS) analysis was performed using an electron microscope (Phenom XL G2, Thermo Fisher Scientific). The EDS analysis shows the elements that are present in the microscale magnetic array. A larger structure was used to extensively analyze the sample, where a single layer of microfluidic device was fabricated with the injected microscale magnet and a low intensity corona treatment was subjected to the PDMS layer and the glass slide. The low intensity bonding ensures that the PDMS layer can be peeled away from the glass slide, which removes the surrounding PDMS and leaves the cured NdFeB-PDMS mixture on the glass slide. This provides a direct contact between the cured NdFeB-PDMS mixture and electron spectrometer and increases the accuracy of the EDS analysis. Table 1 shows the presence of elements of micromagnet. Carbon was disabled in the analysis because the magnet is organic and carbon contains similar atomic energy to Boron, which will alter the results of the EDS analysis. Oxygen, Silicon, Boron, Iron and Neodymium were present at the chosen location, where Oxygen and Silicon are present in PDMS while Boron, Iron and Neodymium are found in the neodymium powder.

3. Numerical methods

In this section, simulation methods and a group of experiment are first presented for validation. Due to the complexity of fabrication, the parametric study was conducted through numerical simulations to reveal the effect of magnet angle and width on the mixing performance. The fluid flow in microfluidic channel is considered as incompressible and under steady-state condition, which is governed by the mass and momentum conservation equations written as

$$\rho\frac{\partial \mathbf{u}}{\partial t}+\rho(\mathbf{u}\cdot\nabla)\mathbf{u}=-\nabla p+\eta\nabla^2\mathbf{u}+\mathrm{F_b} \tag{1}$$

$$\nabla\cdot\mathbf{u}=0 \tag{2}$$

where $\mathbf{u}$ represents the velocity vector field inside microfluidic channel, p is the pressure field, ρ is fluid density, η denotes the dynamic viscosity of fluid, and $\mathbf{F}_b$ is the magnetic body force exerted on ferrofluid. The density and viscosity of ferrofluid-water mixture keep changing during the mixing process and can be described by a linear combination of the local ferrofluid and water concentrations, following equations,

$$\rho=c\rho_f+(1-c)\rho_w \tag{3}$$

$$\eta=\eta_f e^{R(1-c)} \tag{4}$$

where c represents the species concentration of ferrofluid; ρ_f and ρ_w are the density of ferrofluid and water, respectively; η_f and η_w are the viscosity of ferrofluid and water, respectively; R refers to viscosity parameter R=ln(η_w/η_f). The conservation of mass flux during the mixing process can be described by convection-diffusion equation,

$$\nabla\cdot(-D\nabla c+c\mathbf{u})=0 \tag{5}$$

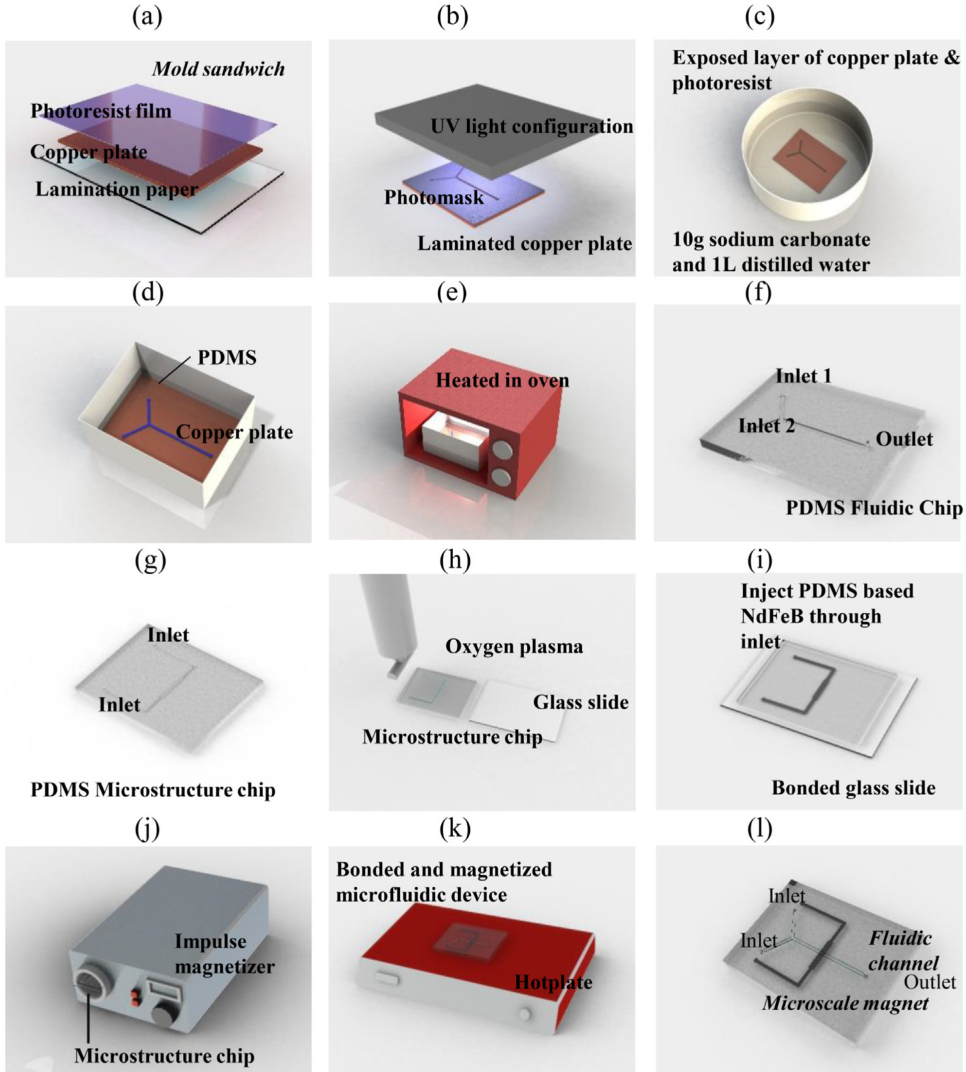

Fig. 2. Fabrication steps of microfluidic device. (a) A mold sandwich is created by pressing a lamination paper, copper plate and photoresist film through an office laminator. (b) A negative photomask is placed on the mold sandwich then they are exposed to ultraviolet light. (c) The covered portion of the exposed photoresist is dissolved in a sodium carbonate solution with a ratio of sodium carbonate and distilled water of 1:100. (d) Degassed PDMS is poured over the master mold in an aluminum case. (e) The case is placed in an oven for 2 hours at 70 °C. (f) The fluidic chip consists of the microfluidic channel with two inlets and one outlet. (g) Steps (a)–(e) are repeated to fabricate the magnet chip. The microstructure for the magnet has two inlets. (h) The magnet chip is temporarily bonded to a glass slide using oxygen plasma treatment to avoid leakage during the filling process. (i) The magnet chip is secured to the glass tightly with pressure; a mixture of neodymium (NdFeB) powder and PDMS is injected into the microstructure. (j) After curing the microscale magnet, an impulse magnetizer was used to indefinitely magnetize the magnetic array. (k) The magnet chip and fluidic chip are attached together using oxygen plasma and heated on a hot plate for 12 h at 120 °C. (l) The two-plane microfluidic chip consists of the fluidic channel on the top layer and magnetic structure on the bottom layer.

where D denotes the diffusion coefficient of commercial water based ferrofluid and is 3.6×10^{-14} m^2/s at room temperature [50], so the time required for pure diffusion to mix two components $t_{diff} = (w_c/2)^2/D$ is much longer than the residence time of fluids inside microfluidic channel, and thus diffusion effect can be neglected compared with convection impact for the mixing performance.

Fig. 4 illustrates the geometry, computational mesh and boundary conditions for the mixing phenomenon occurring in microfluidic channel under the effect of magnetic field in the numerical simulation. The commercial package used in the current studies is COMSOL Multiphysics with the "laminar flow" and "species transport" modules. In summary, for the laminar flow (spf) component, the inlet and outlet of fluidic channel was set as velocity inlet and pressure outlet, respectively. For the diluted species transport (tds) component, the inlet and outlet was set as concentration and outflow, respectively. The channel walls were defined as no-slip walls with zero flux condition in both the laminar flow and diluted species transport components. The boundary condition of magnet was set as magnetic flux conservation B.C. and the magnetic field generated by the magnet was calculated first and then imported into the flow transport model via a one-way coupling approach. Our previous single layer mixer coupled with a magnetic field was calculated with a Finite Element Method Magnetics (FEMM) open-source code [24], while in the current work magnetic, fluid flow and species fields were strongly coupled and integrated for the microfluidic channel.

To be more specific, the complete computational model consists of three different modules coupled to simulate the laminar flow, species transport and magnetohydrodynamics during the mixing process in the microfluidic channel. Fig. 3(a) shows the computational domain used in the current study, which includes the microfluidic channel and a magnetic bar laid beneath the channel perpendicular to the flow direction in the channel. It should

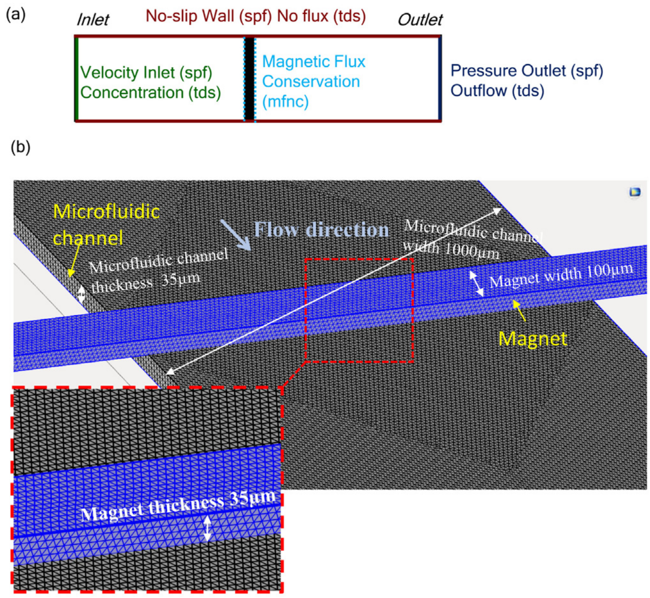

Fig. 3. Boundary condition (B.C.) and geometry of numerical simulation. (a) B.C. for flow field and species transport phenomenon. (b) Geometry and meshes for fludic channel and magnet.

be noted that both Fig. 3 show a zoomed-in portion of the channel near the center region with the magnetic bar included in the view, instead of showing the complete view of the microfluidic system. For the initial condition, the upper half of the channel is filled with distilled water, and the lower half of the channel is filled with ferrofluid. For the fluid flow boundary conditions (B.C.), a velocity inlet B.C. is used on the left-hand-side end of the channel for both the water and ferrofluid with the same flow rate. Both upper and lower boundaries adopt a no-slip wall B.C. with no flow penetration through the boundary. For the right-hand-side end of the microchannel, a pressure outlet B.C. is used with the atmospheric pressure prescribed. With regards to species transport, an outflow B.C. is adopted for the species advected out of the domain by local velocities. For magnetic field calculations, the magnetic flux conservation B.C. is applied at the interface between the magnetic bar and the fluids. Typically the Reynolds numbers for microfluidic applications are much smaller than 1, $Re \sim O(\ll 1)$, due to the low velocities and small scales being operated on. Therefore, a laminar model was applied without using any turbulence model in the simulations for the current work. Good convergences were found in all the case studies performed in this work with calculation error between 10^{-13} to 10^{-14}. Because of the nature of laminar flow with a rather small Reynolds number as found in the current work, no complex vortex structure evolutions were found during experiment or by numerical simulations.

4. Results and discussion

In this section, the effect of total flow rate on mixing performance will be discussed by both simulation and experiments, and the results suggest a very good agreement. This validation provides solid fundamental support to simulate the effect of magnet angle and width on mixing performance between ferrofluid and distilled water, which has been widely recognized as a time and cost efficient way to use validated computational model for parametric study as a useful tool to gain better understanding about the mixing

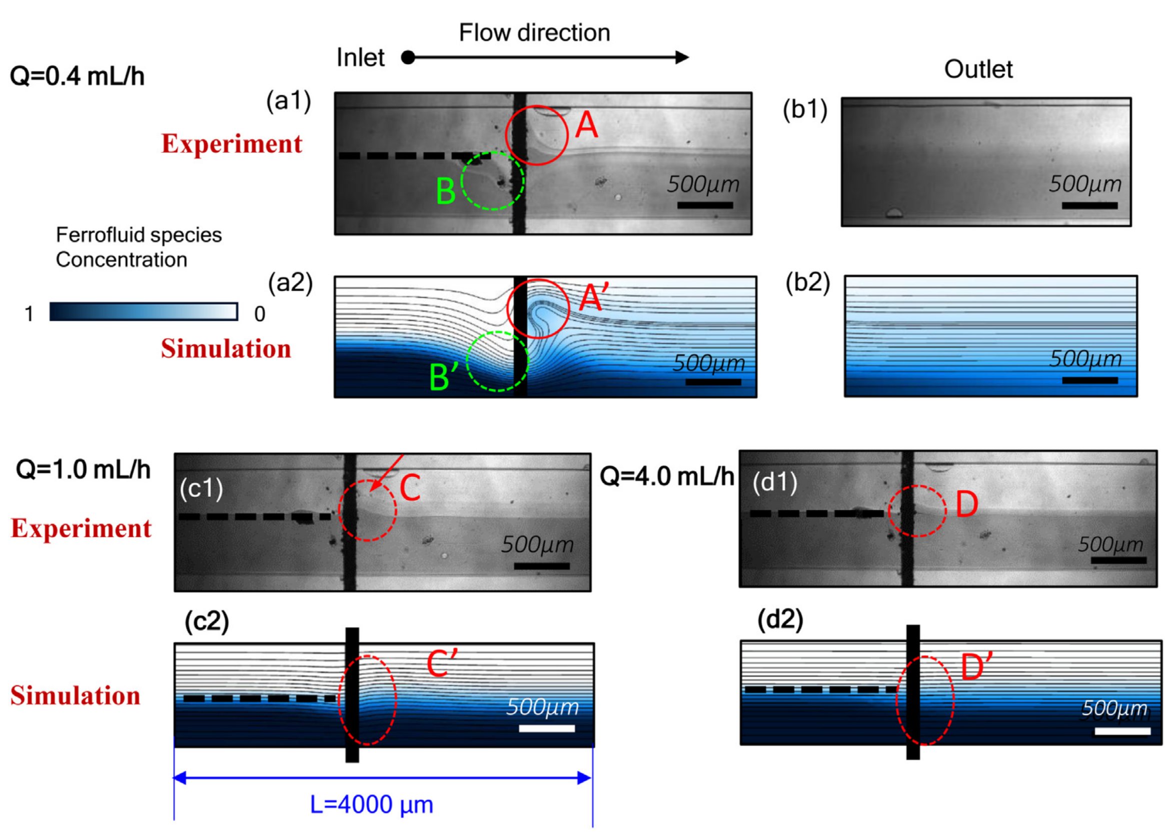

Fig. 4. (a1) and (b1) are the experimental distribution of ferrofluid at inlet and outlet of microfluidic channel when total flow rate $Q = 0.4$ mL/h. (a2) and (b2) are the simulated results corresponding to (a1) and (b1), respectively. (c) and (d) are the experimental and simulation results when total flow rate $Q = 1.0$ mL/h and $Q = 4.0$ ml/h, respectively. The angle between flow direction and magnet is $\pi/2$ for all the groups. (For interpretation of the references to color in this figure legend, the reader is referred to the web version of this article.)

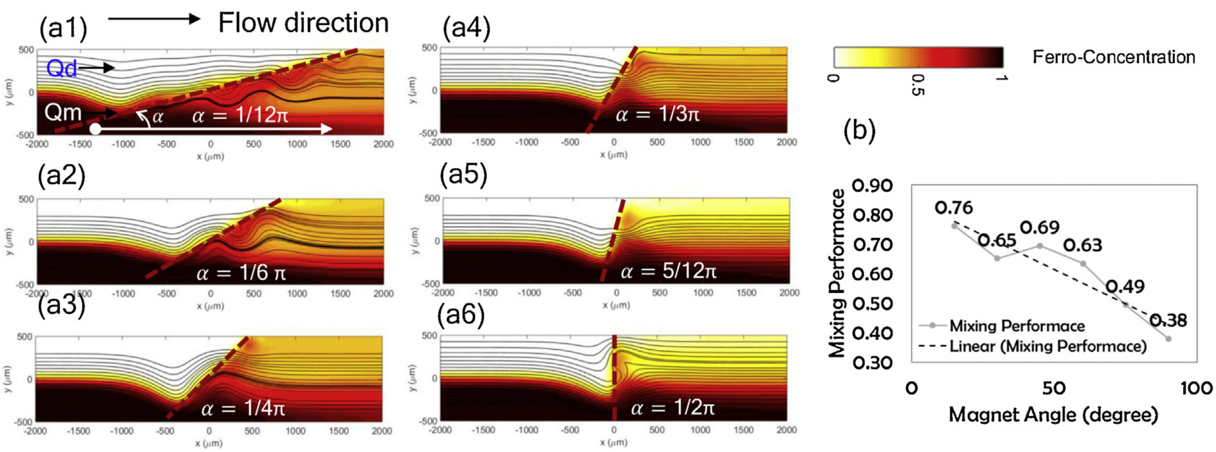

Fig. 5. Effect of inclined angle of magnet on species concentration distribution. (a) Concentration distribution of ferrofluid under various angle α between flow direction and magnet. (b) Effect of inclined angle of magnet on mixing performance corresponding to (a). The total flow rate Q = 0.4 mL/h for all the groups.

phenomenon and overcome the difficulties of complex fabrication process.

4.1. Effect of total flow rate on mixing efficiency and experimental validation

Fig. 4(a) and (b) compare the ferrofluid distributions between experimental observation and the numerical simulation results both at the central channel region (Fig. 4(a1) and 4(a2)) and near the channel outlet (Fig. 4(b1) and 4(b2)) when total flow rate Q = 0.4 mL/h. It is clear that mixing is enhanced towards the channel outlet between water and ferrofluids via passing the magnetic bar. A convex meniscus is observed from experiment measurement in Fig. 4(a1) with a slight downward depression of the interface between the two species before flow reaches the magnetic bar, indicated by region B in the dashed circle in Fig. 4(a1) as compared with the interface from upstream (highlighted by the horizontal dashed line). This phenomenon is also successfully predicted by the numerical simulation as shown by zone B' in Fig. 4(a2). The streamlines in the lower channel region suggest that flow is converging close to the magnetic bar, indicating a higher-velocity accelerating flow towards the magnetic bar because of the attracting magnetic force. A sharp upward jump of the water-ferrofluid interface is then observed to occur within the width of the magnetic bar, and the streamlines in lower channel region change direction from being parallel to the channel walls to almost perpendicular to the upstream interface (dashed horizontal line in Fig. 4a1). This upward burst of flow stream causes the ferrofluid to be immediately advected to the upper channel area (indicated by zone A' in the dashed circle in Fig. 4a2), which overcomes the laminar mass diffusion limitation of the parallel flows if without the magnetic bar. The fundamental mechanism that induces the upward stream which improves mixing of water and ferrofluid therefore resides in the relative strength of the local magnetic force over the flow momentum. [51]. As flow rate increases in the microchannel, the relative significance of the external magnetic field decreases hence lessens mixing. Fig. 4(c) and (d) compare the interfacial phenomenon between ferrofluid and water when the flow passes by the magnet under higher channel flow rates, at 1.0 mL/h and 4.0 mL/h respectively, and it is found the magnetic-field-induced cross-flow perturbation is light and thus weak mixing between two fluids because the higher flow velocity/momentum shortens the residence time of magnetic force acting on ferrofluid. It is observed that when the flow rate is 1.0 mL/h, a slight distortion at the water-ferrofluid interface appears near the magnetic bar (region C in Fig. 4c1), which is confirmed by the simulation results as in region

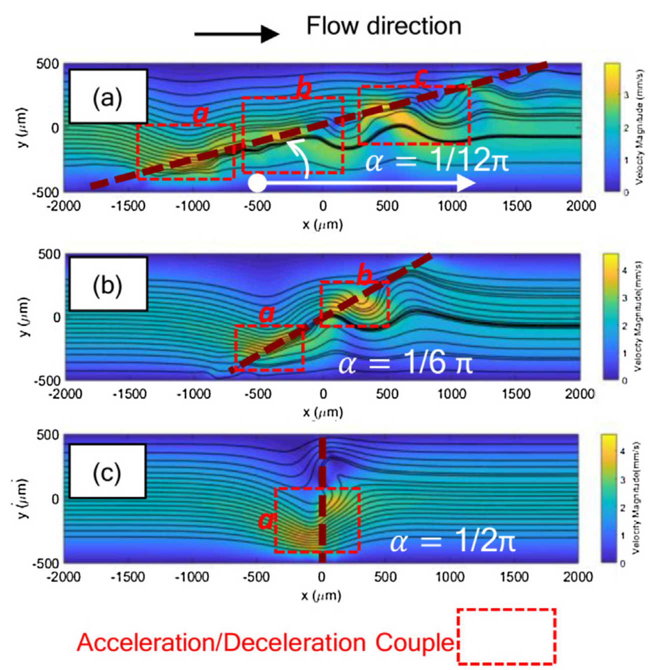

Fig. 6. Velocity magnitude under the effect of various inclined angle of magnet.

C' (Fig. 4c2). When the flow rate is further increased to 4.0 mL/h, a flat, sharp interface between water and ferrofluid is observed with negligible disturbances (region D in Fig. 4d1) by experiment. The same phenomenon is found through numerical simulation in region D' (Fig. 4d2). In both cases with the higher flow rates, the simulated streamlines are almost parallel to the channel walls, suggesting that no significant mixing enhancement is provided by the use of magnetic bars.

4.2. Effect of inclined angle of magnet on mixing efficiency

The effect of inclination angle of the magnetic bar is investigated using the validated model, which is time-saving and cost-saving for performance study and design. Parametric studies are performed with the inclination angle varying between $\pi/12$ and $\pi/2$ relative to the horizontal upstream flow direction. The revolutions of the ferrofluid concentrations and streamlines under different inclination angles are shown in Fig. 5(a1) to (a6). In all cases, the same flow behavior as in Fig. 5 is observed with a convex-shaped meniscus

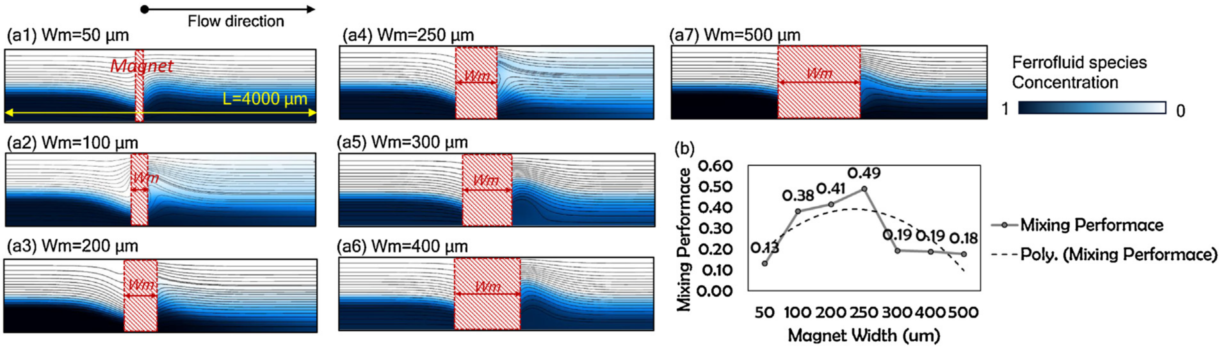

Fig. 7. Effect of magnet width on species concentration distribution of ferrofluid.(a) Species concentration distribution of ferrofluid under various width of magnet w_m. (b) Mixing performance between ferrofluid and water under the effect of magnet with various width. The total flow rate $Q = 0.4$ mL/h for all the groups.

appearing with the water-ferrofluid interface as flow approaches the magnetic bar, inducing an upward deflection of the stream from lower channel towards upper channel area that enhances mixing. However, the level of mixing enhancement varies with the inclination angle. It is shown in Fig. 5 that when the angle is smaller (e.g. $\pi/12$ and $\pi/6$ degrees), the streamline exhibits a wavy pattern following the inclined magnetic bar; while when the inclination angle exceeds $\pi/4$ degrees, the streamlines become smoother with local velocities still pointing towards the direction of inclined magnetic bar. The flow patterns under different inclination angles are illustrated in Fig. 5(b1) to (b6), where the non-uniform velocity distributions are shown in the microchannel. A unique pattern of deceleration followed by acceleration of the flow is commonly found in all cases indicated in the dashed boxes that produces the burst of flow towards the direction of magnetic bar inclination angle and enhances mixing in the microchannel.

It is observed from Fig. 5(a) that the ferrofluid concentration is in general more uniform towards channel outlet with a smaller inclination angle, suggesting better mixing. The species concentration of ferrofluid was extracted from the outlet of microfluidic channel when mixing reaches steady state and the mixing performance was calculated using the following equation,

$$\text{Mixing performance} = 1 - \sqrt{1/N\sum_{i=1}^{n}\left(\frac{c_i - \bar{c}}{\bar{c}}\right)^2} \tag{6}$$

where c_i and $\bar{c}$ represents the species concentration of ferrofluid of each mesh node and mean concentration at the outlet of microfluidic channel. Fig. 5(b) demonstrates the overall effect of magnet angle on the mixing performance between ferrofluid and distilled water. It is found from both simulated results and its trend line that the mixing performance decreases with increasing angle. The degrees of mixing are also quantified and plotted in Fig. 5(b) that shows the decrease of mixing performance with increasing the inclination angle: from 0.8 under the $\pi/12$ angle to 0.4 when the magnetic bar is perpendicular to the streamwise direction. A main reason for this is because of the increased mixing length subjected to advection under smaller inclination angles.

In this work, the effect of the angle between magnet and flow direction was studied using simulation. Fig. 5(a) demonstrates the concentration distribution of ferrofluid under various angle α between flow direction and magnet and Fig. 6(a–c) are the velocity magnitude corresponding to 5 (a). It was found that the mixing performance was the most homogeneous when the angle $\alpha = 1/12\pi$. This can be explained by the acceleration of fluid caused by the magnetic field and force generated by magnet. From the dashed rectangle in Fig. 6, ferrofluid is accelerated when getting close to the magnet while decelerated after flowing past the magnet. From Fig. 6(a) when $\alpha = 1/12\pi$, there are three couples of acceleration and deceleration which means more pushing and mixing of ferrofluid with water and thus better mixing performance. According to mass conservation, this coupled acceleration and deceleration will narrow and widen the distribution width of ferrofluid when it reaches and leaves magnet, respectively. Widening the distribution of ferrofluid means ferrofluid was pushed and mixed with distilled water. Compared with the three acceleration and deceleration couple in Fig. 6(a), when angle $\alpha = 1/6\pi$ (Fig. 6b) and $\alpha = 1/2\pi$ (Fig. 6c), the acceleration-deceleration couples (ADC) are reduced: two ADCs are found for the case with $\alpha = 1/6\pi$ and only one for $\alpha = 1/6\pi$ case. It is observed from the high velocity streaks that the length scale for each of the ADCs in all three cases are approximately the same, around 200–300 µm in width and 400–500 µm in length. The wavy velocity paths in Fig. 6(a–c) also show their directions pointing towards the inclination angles of the magnetic bar in each case. For the practical perspective, smaller inclination angles indicate longer magnets to be fabricated to cover the channel. Due to the scale of the impulse magnetizer, it becomes difficult to fit elongated magnet bars for the magnetization process. Despite of the limitations with manufacturing precision to place small angles, additional difficulties are present to avoid structural failure when manipulating long objects at such a small scale. For the theoretical aspects, another numerical simulation has been performed with a smaller inclination angle of $\pi/24$. Results shows similar mixing performance compared to the case with a $\pi/12$ inclination angle with a mere 1% increase, which indicates a very narrow margin when pursuing smaller inclination angles, thus little benefit in practice with even smaller inclination angle.

4.3. Effect of width of magnet on mixing efficiency

The effect of magnet width on water-ferrofluid mixing is addressed in this section which is greatly beneficial to overcome the complex fabrication process in time-efficient way. Fig. 7(a) demonstrates the concentration distribution of ferrofluid under different widths of magnet w_m, ranging from $w_m = 50\,\mu$m to $w_m = 500\,\mu$m. When the magnet width is below $w_m = 250\,\mu$m, an obvious enhancement of the mixing performance is observed with the increase of the magnet width. If the magnet width is above $w_m = 250\,\mu$m, however, little impact is found by the magnet width. The species concentration of ferrofluid was extracted at the outlet. The corresponding mixing performance was calculated according to Eq. (6) and plotted in Fig. 7(b), which shows a peak at the magnet width of $w_m = 250\,\mu$m with a mixing degree of 0.49, followed by a sudden drop of the mixing level to 0.19 for the widths higher than $w_m = 250\,\mu$m. It was found that the mixing performance increases as the magnet width increases from $w_m = 50\,\mu$m to $w_m = 250\,\mu$m while decreases when magnet width is wider than $w_m = 250\,\mu$m. To examine the details of local flow behavior

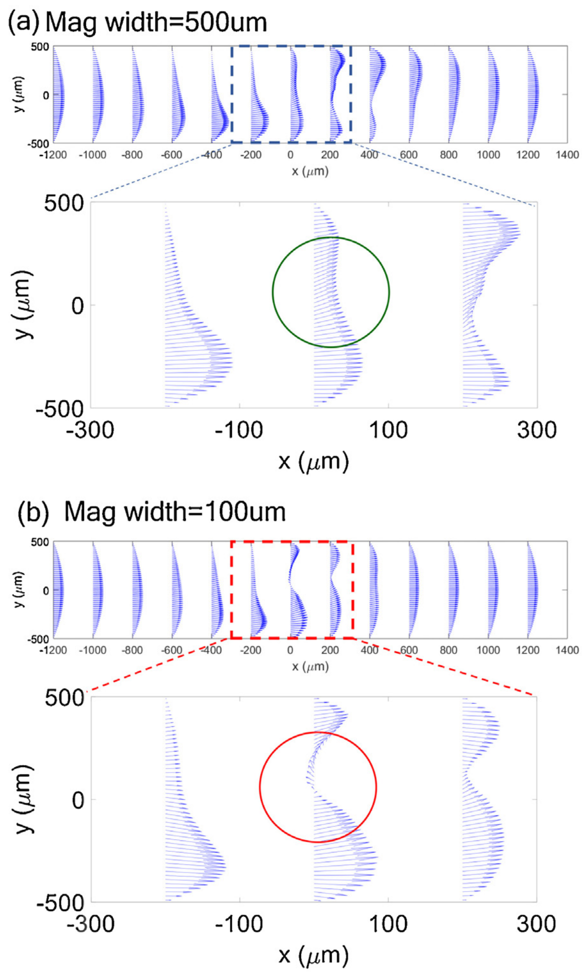

Fig. 8. (a) Mixing performance between ferrofluid and water under the effect of magnet with various width. Flow field in microfluidic channel when magnet width is (a) $w_m = 500\,\mu\text{m}$ and (b) $w_m = 100\,\mu\text{m}$, respectively. (For interpretation of the references to color in this figure legend, the reader is referred to the web version of this article.)

to explain the trend of mixing performance, Fig. 8 demonstrates the flow field in microfluidic channel when magnet width is (a) $w_m = 500\,\mu\text{m}$ and (b) $w_m = 100\,\mu\text{m}$, respectively. With a magnetic bar width of 500 μm (indicated by the dashed box in Fig. 8a), it is clearly shown that ferrofluid velocity in the lower channel region is accelerated near $x = -200\,\mu\text{m}$, then slows down due to combined effects of deceleration by magnetic force and shear at the water-ferrofluid interface (at $x = 0\,\mu\text{m}$), and eventually fluid velocity in the upper layer is accelerated because of the ADC effect ($x = 200\,\mu\text{m}$). It is worth noting that velocity profiles in the case with a magnetic bar width of 500 μm all point towards the streamwise direction, despite of the upward velocity component. However, it is evident that reverse flow is present (indicated by circle in Fig. 8b) when $w_m = 100\,\mu\text{m}$, which decreases the streamwise velocity and thus lowers the local Peclet number so that it allows more laminar diffusion to take place along the water-ferrofluid interface. Therefore, with a higher upward momentum because of mass conservation combined with a reduced local *Pe* number, the distribution width of ferrofluid and resultant mixing performance is increased for the case with a magnetic bar width of 100 μm.

5. Conclusion

This study presented a magnetism based micromixer and conducted a comprehensive discussion of mixing performance under the effect of flow rate, magnet angle and width. The mixing phenomenon of base case (angle between magnet and flow direction $\alpha = 1/2\pi$ and magnet width $w_m = 100\,\mu\text{m}$) was simulated by COMSOL Multiphysics and validated by experiment. The results of mixing simulation and experiment under various total flow rates show very good agreement, so the simulation methods were applied to discuss the effect of magnet placement angle and magnet width on the mixing performance, which is time- and cost-efficient, and overcome the difficulties and barrier of complicated fabrication process. It was found that the mixing performance was the most homogeneous when the angle $\alpha = 1/12\pi$ because of the acceleration-deceleration couples (ADC) and mass conservation law. It was also found that the mixing performance increases as the magnet width increases from $w_m = 50\,\mu\text{m}$ to $w_m = 250\,\mu\text{m}$ while decreases when magnet width is wider than $w_m = 250\,\mu\text{m}$. This can be explained by the reverse flow which decreases the streamwise velocity and thus lowers the local Peclet number so that it allows more laminar diffusion to take place along the water-ferrofluid interface. Therefore, the micromixer with placement angle $\alpha = 1/12\pi$ and magnet width $w_m = 250\,\mu\text{m}$ is a preferable design to enable rapid mixing using compact magnetic field and thus provides great potential to be utilized in biological application because no harmful Joule heat is generated in the proposed device. For an overall optimization of the process, more parameters need to be considered and experimented such as the widths of microfluidic channel and the magnet bar, throughputs, magnetization strength, on top of the magnet inclination angle. The idea of using optimization schemes such as a box behnken design or some other design of experiments (DOE) methods will serve a great tool for future overall process optimization.

Author contributions

Ran Zhou: Conceptualization of this study, methodology, investigation and supervision
Athira Surendran: Device fabrication, experiment conduction, results analysis
Jingyang Wang: Device fabrication and experiment conduction

Declaration of interests

The authors declare that they have no known competing financial interests or personal relationships that could have appeared to influence the work reported in this paper.

Declaration of Competing Interest

The authors report no declarations of interest.

Acknowledgement

The authors would like to thank NSF CMMI No.1920039 for supporting Scanning Electron Microscope (SEM) equipment for materials validation. The authors would also like to thank Purdue University Northwest Internal Research Grants for the support of research supplies.

References

[1] G.M. Whitesides, The origins and the future of microfluidics, Nature 442 (2006) 368–373.
[2] P. Tabeling, Introduction to Microfluidics, OUP Oxford, 2005.
[3] H. Bruus, Theoretical Microfluidics, vol. 18, Oxford University Press, Oxford, 2008.
[4] N.-T. Nguyen, S.T. Wereley, S.A.M. Shaegh, Fundamentals and Applications of Microfluidics, Artech House, 2019.
[5] S.A.M. Shaegh, A. Pourmand, M. Nabavinia, H. Avci, A. Tamayol, P. Mostafalu, H.B. Ghavifekr, E.N. Aghdam, M.R. Dokmeci, A. Khademhosseini, et al., Rapid

prototyping of whole-thermoplastic microfluidics with built-in microvalves using laser ablation and thermal fusion bonding, Sens. Actuators B: Chem. 255 (2018) 100–109.
[6] S. Atabakhsh, S.J. Ashtiani, Thermal actuation and confinement of water droplets on paper-based digital microfluidics devices, Microfluid. Nanofluid. 22 (4) (2018) 1–9.
[7] S.O. Catarino, R.O. Rodrigues, D. Pinho, J.M. Miranda, G. Minas, R. Lima, Blood cells separation and sorting techniques of passive microfluidic devices: from fabrication to applications, Micromachines 10 (9) (2019) 593.
[8] M. Tang, G. Wang, S. Kong, H.P. Ho, A review of biomedical centrifugal microfluidic platforms, Micromachines 7 (2) (2016) 26.
[9] A. Dalili, E. Samiei, M. Hoorfar, A review of sorting, separation and isolation of cells and microbeads for biomedical applications: microfluidic approaches, Analyst 144 (1) (2019) 87–113.
[10] E.K. Sackmann, A.L. Fulton, D.J. Beebe, The present and future role of microfluidics in biomedical research, Nature 507 (7491) (2014) 181–189.
[11] E. Brouzes, M. Medkova, N. Savenelli, D. Marran, M. Twardowski, J.B. Hutchison, J.M. Rothberg, D.R. Link, N. Perrimon, M.L. Samuels, Droplet microfluidic technology for single-cell high-throughput screening, Proc. Natl. Acad. Sci. USA 106 (34) (2009) 14195–14200.
[12] J. Ahn, J. Ko, S. Lee, J. Yu, Y. Kim, N.L. Jeon, Microfluidics in nanoparticle drug delivery; from synthesis to pre-clinical screening, Adv. Drug Deliv. Rev. 128 (2018) 29–53.
[13] A. Burklund, A. Tadimety, Y. Nie, N. Hao, J.X. Zhang, Advances in diagnostic microfluidics, Adv. Clin. Chem. 95 (2020) 1–72.
[14] F. Fontana, M.P. Ferreira, A. Correia, J. Hirvonen, H.A. Santos, Microfluidics as a cutting-edge technique for drug delivery applications, J. Drug Deliv. Sci. Technol. 34 (2016) 76–87.
[15] C.J. Kastrup, J.Q. Boedicker, A.P. Pomerantsev, M. Moayeri, Y. Bian, R.R. Pompano, T.R. Kline, P. Sylvestre, F. Shen, S.H. Leppla, et al., Spatial localization of bacteria controls coagulation of human blood by 'quorum acting', Nat. Chem. Biol. 4 (12) (2008) 742–750.
[16] R. Riahi, A. Tamayol, S.A.M. Shaegh, A.M. Ghaemmaghami, M.R. Dokmeci, A. Khademhosseini, Microfluidics for advanced drug delivery systems, Curr. Opin. Chem. Eng. 7 (2015) 101–112.
[17] J.V. Pagaduan, V. Sahore, A.T. Woolley, Applications of microfluidics and microchip electrophoresis for potential clinical biomarker analysis, Anal. Bioanal. Chem. 407 (23) (2015) 6911–6922.
[18] Y. Yang, Y. Chen, H. Tang, N. Zong, X. Jiang, Microfluidics for biomedical analysis, Small Methods 4 (4) (2020) 1900451.
[19] T. Yang, Y.-C. Wang, C.-F. Shen, C.-M. Cheng, Point-of-care rna-based diagnostic device for covid-19, Diagnostics (2020).
[20] C.M. Pandey, S. Augustine, S. Kumar, S. Kumar, S. Nara, S. Srivastava, B.D. Malhotra, Microfluidics based point-of-care diagnostics, Biotechnol. J. 13 (1) (2018) 1700047.
[21] S. Sharma, J. Zapatero-Rodríguez, P. Estrela, R. O'Kennedy, Point-of-care diagnostics in low resource settings: present status and future role of microfluidics, Biosensors 5 (3) (2015) 577–601.
[22] L. Zhang, B. Ding, Q. Chen, Q. Feng, L. Lin, J. Sun, Point-of-care-testing of nucleic acids by microfluidics, TrAC Trends Anal. Chem. 94 (2017) 106–116.
[23] G.S. Jeong, S. Chung, C.-B. Kim, S.-H. Lee, Applications of micromixing technology, Analyst 135 (3) (2010) 460–473.
[24] R. Zhou, A.N. Surendran, M. Mejulu, Y. Lin, Rapid microfluidic mixer based on ferrofluid and integrated microscale ndfeb-pdms magnet, Micromachines 11 (1) (2020) 29.
[25] E.M. Miller, A.R. Wheeler, A digital microfluidic approach to homogeneous enzyme assays, Anal. Chem. 80 (5) (2008) 1614–1619.
[26] C.-Y. Lee, G.-B. Lee, J.-L. Lin, F.-C. Huang, C.-S. Liao, Integrated microfluidic systems for cell lysis, mixing/pumping and dna amplification, J. Micromech. Microeng. 15 (6) (2005) 1215.
[27] D.E. Hertzog, B. Ivorra, B. Mohammadi, O. Bakajin, J.G. Santiago, Optimization of a microfluidic mixer for studying protein folding kinetics, Anal. Chem. 78 (13) (2006) 4299–4306.
[28] A.S. Kane, A. Hoffmann, P. Baumgartel, R. Seckler, G. Reichardt, D.A. Horsley, B. Schuler, O. Bakajin, Microfluidic mixers for the investigation of rapid protein folding kinetics using synchrotron radiation circular dichroism spectroscopy, Anal. Chem. 80 (24) (2008) 9534–9541.
[29] B. Ivorra, D.E. Hertzog, B. Mohammadi, J.G. Santiago, Semi-deterministic, genetic algorithms for global optimization of microfluidic protein-folding devices, Int. J. Numer. Methods Eng. 66 (2) (2006) 319–333.
[30] C.-Y. Lee, C.-L. Chang, Y.-N. Wang, L.-M. Fu, Microfluidic mixing: a review, Int. J. Mol. Sci. 12 (5) (2011) 3263–3287.
[31] Y.K. Suh, S. Kang, A review on mixing in microfluidics, Micromachines 1 (3) (2010) 82–111.
[32] E.A. Mansur, Y. Mingxing, W. Yundong, D. Youyuan, A state-of-the-art review of mixing in microfluidic mixers, Chin. J. Chem. Eng. 16 (4) (2008) 503–516.
[33] W. Huang, Transverse jet in supersonic crossflows, Aerosp. Sci. Technol. 50 (2016) 183–195.
[34] W. Huang, Mixing enhancement strategies and their mechanisms in supersonic flows: a brief review, Acta Astronaut. 145 (2018) 492–500.
[35] W. Huang, Z.-B. Du, L. Yan, Z.-X. Xia, Supersonic mixing in airbreathing propulsion systems for hypersonic flights, Prog. Aerosp. Sci. 109 (2019) 100545.
[36] R.-J. Yang, H.-H. Hou, Y.-N. Wang, L.-M. Fu, Micro-magnetofluidics in microfluidic systems: a review, Sens. Actuators B: Chem. 224 (2016) 1–15.
[37] V. Hessel, H. Löwe, F. Schönfeld, Micromixers – a review on passive and active mixing principles, Chem. Eng. Sci. 60 (8–9) (2005) 2479–2501.
[38] G. Cai, L. Xue, H. Zhang, J. Lin, A review on micromixers, Micromachines 8 (9) (2017) 274.
[39] H. Shi, K. Nie, B. Dong, L. Chao, F. Gao, M. Ma, M. Long, Z. Liu, Mixing enhancement via a serpentine micromixer for real-time activation of carboxyl, Chem. Eng. J. 392 (2020) 123642.
[40] M. Nazari, S. Rashidi, J.A. Esfahani, Mixing process and mass transfer in a novel design of induced-charge electrokinetic micromixer with a conductive mixing-chamber, Int. Commun. Heat Mass Transf. 108 (2019) 104293.
[41] M.R. Rasouli, M. Tabrizian, An ultra-rapid acoustic micromixer for synthesis of organic nanoparticles, Lab Chip 19 (19) (2019) 3316–3325.
[42] S.S.M. Ajarostaghi, M.A. Delavar, S. Poncet, Thermal mixing, cooling and entropy generation in a micromixer with a porous zone by the lattice boltzmann method, J. Therm. Anal. Calorim. 140 (3) (2020) 1321–1339.
[43] D. Nouri, A. Zabihi-Hesari, M. Passandideh-Fard, Rapid mixing in micromixers using magnetic field, Sens. Actuators A: Phys. 255 (2017) 79–86.
[44] Y. Wang, J. Zhe, B.T. Chung, P. Dutta, A rapid magnetic particle driven micromixer, Microfluid. Nanofluid. 4 (5) (2008) 375–389.
[45] C. Liosis, E.G. Karvelas, T. Karakasidis, I.E. Sarris, Numerical study of magnetic particles mixing in waste water under an external magnetic field, J. Water Supply: Res. Technol.-AQUA 69 (3) (2020) 266–275.
[46] C. Kumar, M. Hejazian, C. From, S.C. Saha, E. Sauret, Y. Gu, N.-T. Nguyen, Modeling of mass transfer enhancement in a magnetofluidic micromixer, Phys. Fluids 31 (6) (2019) 063603.
[47] M. Hejazian, N.-T. Nguyen, Magnetofluidic concentration and separation of non-magnetic particles using two magnet arrays, Biomicrofluidics 10 (4) (2016) 044103.
[48] Z. Zhang, R. Zhou, D. Brames, C. Wang, A low-cost fabrication system for manufacturing soft-lithography microfluidic master molds, Micro Nanosyst. 7 (2015) 4–12.
[49] R. Zhou, Q. Yang, F. Bai, J.A. Werner, H. Shi, Y. Ma, C. Wang, Fabrication and integration of microscale permanent magnets for particle separation in microfluidics, Microfluid. Nanofluid. 20 (7) (2016) 1–12.
[50] T. Zhu, D.J. Lichlyter, M.A. Haidekker, L. Mao, Analytical model of microfluidic transport of non-magnetic particles in ferrofluids under the influence of a permanent magnet, Microfluid. Nanofluid. 10 (6) (2011) 1233–1245.
[51] R. Zhou, A.N. Surendran, Study on micromagnets induced local wavy mixing in a microfluidic channel, Appl. Phys. Lett. 117 (13) (2020) 132408.

Biographies

Dr. Ran Zhou is an Assistant Professor from Department of Mechanical and Civil Engineering at Purdue University Northwest.

Athira N. Surendran was a master student from Department of Mechanical and Civil Engineering at Purdue University Northwest. Her thesis topic is development of fabrication platform for microfluidic devices and experimental study of magnetic mixing and separation.

Jingyang Wang is a graduate student from Department of Mechanical and Civil Engineering at Purdue University Northwest.